The lag–luminosity correlation in time-resolved episodes of long gamma-ray bursts

By
Samuel J. Kowash

A THESIS

submitted to

Oregon State University

University Honors College

in partial fulfillment of
the requirements for the
degree of

Honors Baccalaureate of Science in Physics
(Honors Scholar)

Honors Baccalaureate of Science in Mathematics
(Honors Scholar)

Presented May 16, 2016
Commencement June 2016

AN ABSTRACT OF THE THESIS OF

Samuel J. Kowash for the degree of Honors Baccalaureate of Science in Physics and Honors Baccalaureate of Science in Mathematics presented on May 16, 2016. Title: The lag–luminosity correlation in time-resolved episodes of long gamma-ray bursts

Abstract approved:

Davide Lazzati

We present an analysis of the relationship between spectral lag and luminosity in time-resolved segments of long gamma-ray bursts detected by BATSE, an experiment aboard the Compton Gamma Ray Observatory satellite. For full bursts, there is a well-established correlation between the lag, which is easily computed, and the total burst luminosity, which is often difficult to determine. We investigate the possibility that this lag–luminosity relationship extends to intervals and pulses within a burst. This is motivated by the complex time profile of many bursts, which can involve high variability ("spikiness") and distinct multi-pulse structures.

To measure time-resolved lags, we perform cross-correlation analysis on slices of light curves selected with a Gaussian filter tuned either to isolate distinct pulses where present or otherwise partition the burst evenly. Taking peak count rate as a proxy for luminosity, we fit a power-law to the lag–luminosity data of slices within each burst. In a sample of 31 bursts, we find a weighted mean power law index of -0.117 ± 0.052, with a more significant mean of -0.455 ± 0.071 appearing in the subset of bursts with distinguishable pulse events. We also observe a strong positive correlation in a set of bursts with precursor events, but refrain from drawing conclusions due to the size of that sample.

Our results suggest the possibility of a time-resolved lag–luminosity correlation, especially in the population of bursts consisting of multiple distinct emission events. The power of this evidence is limited by sample size, but encourages further work on a larger sample of more recent data. If it exists, such an intra-burst lag correlation would help validate the correlation across full bursts, since it is less affected by selection effects.

Key Words: spectral lag, gamma-ray bursts, high-energy astrophysics

Corresponding e-mail address: kowashs@oregonstate.edu

The lag–luminosity correlation in time-resolved episodes of long gamma-ray bursts

By
Samuel J. Kowash

A THESIS

submitted to

Oregon State University

University Honors College

in partial fulfillment of
the requirements for the
degree of

Honors Baccalaureate of Science in Physics
(Honors Scholar)

Honors Baccalaureate of Science in Mathematics
(Honors Scholar)

Presented May 16, 2016
Commencement June 2016

Honors Baccalaureate of Science in Physics and Honors Baccalaureate of Science in Mathematics project of Samuel J. Kowash presented on May 16, 2016

APPROVED:

Davide Lazzati, Mentor, representing Physics

David Roundy, Committee Member, representing Physics

Kathryn Hadley, Committee Member, representing Physics

Toni Doolen, Dean, Oregon State University Honors College

I understand that my project will become part of the permanent collection of Oregon State University Honors College. My signature below authorizes release of my project to any reader upon request.

Samuel J. Kowash, Author

Contents

1 Background **2**
- 1.1 GRB detection . . . 2
  - 1.1.1 BATSE and BeppoSAX . . . 2
- 1.2 Burst characteristics . . . 2
  - 1.2.1 Distribution . . . 2
  - 1.2.2 Duration . . . 3
  - 1.2.3 Energy . . . 3
  - 1.2.4 Progenitors . . . 3
- 1.3 Spectral Lag . . . 3

2 Methods **5**
- 2.1 Burst selection . . . 5
- 2.2 Data preparation . . . 6
  - 2.2.1 Data format . . . 6
  - 2.2.2 Slice formation . . . 6
- 2.3 Analysis . . . 8
  - 2.3.1 Cross-correlation . . . 8
  - 2.3.2 Curve fitting . . . 9
  - 2.3.3 Monte Carlo error estimation . . . 10
  - 2.3.4 Slope fitting . . . 11

3 Results and Discussion **12**
- 3.1 Weighted mean . . . 12
- 3.2 Conclusions . . . 15

List of Figures

1.1 Illustrations of global and time-resolved lags; ch3 is high-energy, ch1 is low . 4

2.1 Typical FRED light curve 5
2.2 Typical light curve lacking distinct pulses 6
2.3 Light curve of pulsed GRB 940217 before and after Gaussian filter 7
2.4 Cross-correlation of second pulse in GRB 940217 with fit line 9

3.1 Scatter plot of computed lag slopes with uncertainty 13
3.2 Histogram of computed lag slope values 13

Introduction

About once every three days, an orbital observatory such as *Swift* detects a massive emission of very high energy photons from somewhere in the sky. These events, known as gamma-ray bursts (GRBs), were first detected in 1967 by US satellites intended to monitor nuclear treaty compliance, and have been objects of great interest in astrophysics research since then. Because gamma radiation defies imaging (it tends to penetrate lenses rather than refract in them), simply localizing bursts in the sky, much less the universe, was an early research challenge. It has since been found that all known bursts originate in other galaxies, so the amount of radiation detected on Earth implies that GRBs are among the most luminous objects in the universe. This makes them excellent tools for probing the early universe, and some of the most distant known objects are GRBs. These bursts can give us indications of early star-forming galaxies which are not otherwise detectable.

Because of its utility in deriving information about GRB progenitors, the spectral behavior of bursts, especially evolution over time, is of significant interest. In many bursts it is found that high-energy photons precede low-energy photons, so that the shape of the signal in a low energy range is simply a translation of the higher-energy parts of the signal. The magnitude of this translation is known as the spectral lag, and is easily measured from radiation count data by a method known as cross-correlation analysis. Because the measurement is so convenient, correlations between spectral lag and more elusive quantities are highly sought-after. Several past studies [15, 3, 4] have determined and refined a connection between the total spectral lag and the peak luminosity of a burst. However, many gamma-ray bursts consist of several pulses of varying intensity, so measuring the lag over the entire burst may erase the contributions of individual pulses, and it is natural to ask whether such a correlation exists between the lag and luminosity of such pulses within bursts. A few studies [10, 12] have investigated this question, but their methods require knowledge of the redshift of the bursts and compare pulses across different bursts.

In the present work, we investigate the presence of a lag–luminosity correlation across pulses of gamma-ray bursts by a time-resolved cross-correlation method which obviates the need for redshift data by only comparing pulses within a burst and averaging the trend across the whole sample.

Chapter 1

Background

1.1 GRB detection

The *Vela* satellite network was launched in 1963 to monitor Soviet compliance with the Partial Test Ban Treaty. Its mission was (fortunately) uneventful with two exceptions: the politically interesting detection on 22 September, 1979 of a double radiation pulse off Antarctica consistent with a nuclear test, and the scientifically interesting detection on 2 July, 1967 of a massive flash of gamma radiation inconsistent with any known nuclear weapon. This was the first observation of a cosmic gamma-ray burst. Further burst detections eliminated the possibility of terrestrial or local origin, and the first publication on the topic was released in 1973 [11].

1.1.1 BATSE and BeppoSAX

Two instruments were essential in beginning to understand the distribution and origin of many gamma-ray bursts. BATSE, launched in 1991 on NASA's Compton Gamma-Ray Observatory, was a wide-field gamma-ray detector intended in part to determine the spatial origin of bursts. At the time, it was as yet unclear whether bursters were at local, galactic, or cosmological distances. BeppoSAX was an X-ray telescope operated by an Italian–Dutch collaboration which was the first instrument to detect a GRB afterglow [17]. This period of low-energy emission following many bursts offers valuable information about a burst's location, environment, and progenitor.

1.2 Burst characteristics

1.2.1 Distribution

The spatial distribution of gamma-ray bursts was mysterious for much of the early period of research. With very little ability to localize bursts in the sky, it was almost impossible to draw conclusions about their environments or locations. A major advance was made when BATSE observations demonstrated that the angular distribution of observed bursts is uniform, with no dipole or quadrupole moments [7]. This effectively ruled out local or Milky Way origins for bursts, since we would expect a concentration in the galactic plane in that case. Alternative hypotheses were put forward, including a spherical halo of bursters surrounding the galaxy, but few were compelling compared to models placing GRBs at cosmological scales. However, the question of distance scale was not entirely settled until

BeppoSAX began detecting X-ray afterglows, which enabled optical afterglow observation and thereby redshift measurements which placed GRBs in distant host galaxies [8].

1.2.2 Duration

The duration of a gamma-ray burst is characterized by a metric called the T_{90}, which is the time required to integrate the middle 90% of the radiation counts detected for a given event. By this measurement, the distribution of durations is strongly bimodal, dividing the population into long ($T_{90} > 2$ s) and short ($T_{90} < 2$ s) bursts [8]. Short bursts tend to have harder spectra than long bursts, and may originate from very different events. Although some papers [3] have investigated the spectral lag of short bursts, it is in general difficult to measure precisely, especially from relatively low-resolution BATSE data. Thus, we focus here on long bursts.

1.2.3 Energy

Given the cosmological distances to bursters, the GRB photon fluxes detected from Earth imply enormous peak luminosities, estimated to be on or greater than the order of 10^{53} $\frac{\text{ergs}}{\text{s}}$ for many bursts [8]. This magnitude firmly establishes GRBs as the most luminous known astrophysical events. However, the high variability in GRB signals implies a very small source region (hundreds of kilometers), which places great demands on any proposed progenitor. Current theories suggest relativistic jets rather than isotropic emission, which reduces the energy requirement considerably (to the 10^{51} erg range), but the energy density required remains massive and limits the possible progenitors for GRBs [8].

1.2.4 Progenitors

Stellar death and remnants have been implicated in GRB production since BATSE and BeppoSAX observations confirmed that bursts originate at cosmological distances. GRBs were seen to be more concentrated in young star-forming regions, and the energy scale of some supernovae is consistent with that of gamma-ray bursts. However, no evidence directly linked the two events until SN 1998bw was observed coincident with GRB 980425 [18]. Subsequent observations connected many long GRBs to supernovae, and recent models focus on jets powered by matter accreting onto a rotating proto-neutron star formed in a core-collapse supernova [8].

No short bursts, however, have been associated with supernovae to date, so they are expected to originate from a different type of system. The core elements of the emission remain the same in short burst models: infalling matter in a dense, rotating system generates collimated relativistic outflows along the axis of rotation. In short bursts, the system is thought to be a merging binary consisting of two neutron stars or a neutron star and a black hole [18]. These systems have extremely complex dynamics, but as computational power grows it is increasingly feasible to simulate toy models or limited properties of mergers and jet production, which will hopefully shed light on GRB generation.

1.3 Spectral Lag

Spectral evolution in gamma-ray bursts carries key clues about progenitors and their environments and has thus been the focus of considerable research. Spectral lag is one facet of

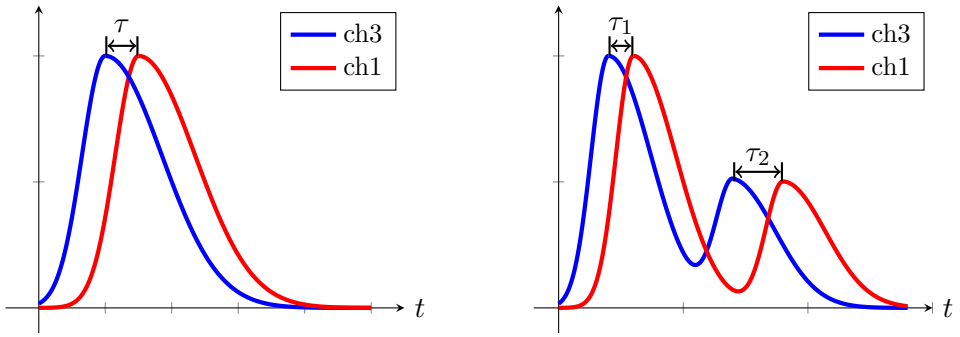

(a) Schematic illustration of spectral lag in single-pulse burst

(b) Schematic illustration of time-resolved lag

Figure 1.1: Illustrations of global and time-resolved lags; ch3 is high-energy, ch1 is low

this evolution. Cheng et al. [6] found that low-energy emission patterns often followed high-energy emission with a time delay in a sample of BATSE light curves; the size of this delay is known as the spectral lag of the burst (represented in Figure 1.1a). Because lag is easy to measure, any robust correlation between it and more difficult properties is a valuable tool. Norris et al. [15] demonstrated a power-law relationship between lag and peak luminosity, then subsequently developed a method based on this correlation to estimate redshift and luminosity from spectral lag [14].

Since Norris, several papers have expanded the study of lags and refined the lag–luminosity correlation. Margutti et al. [13] found lag behavior in X-ray flares associated to GRBs, suggesting similar emission mechanisms for both events. As redshift data became available for many more bursts (thanks largely to Swift), Ukwatta et al. [16] measured lags between energy bands adjusted to the reference frame of the burster and determined a more robust lag–luminosity correlation than Norris. When possible, source-frame methods are now the standard, but BATSE data do not permit this.

Short GRBs were historically difficult subjects for lag analysis due to low instrument resolution, but the advent of the Swift and Fermi platforms has enabled lag studies involving short bursts. Zhang et al. [19] proposed that the lag–luminosity correlation extends to short bursts, although Bernardini et al. [3] found short GRB lags almost all negligible. The latter study further observed that the inclusion of bursts with negative lag (sometimes considered spurious) weakens the lag–luminosity correlation considerably.

Because of the complex structure of GRB light curves, which can include multiple distinct pulses with various luminosities, it is natural to ask 1) whether different pulses have distinct lags (represented in Figure 1.1b) or whether the property is global, and 2) whether the lag–luminosity correlation holds for episodes within bursts. It has been shown that pulses can certainly have lags distinct from the total lag, but the second question is in dispute and the focus of the present work. Chen et al. [5] computed lags for some pulses and found no universal trend in pulse lags, either temporal or a luminosity correlation. Jia et al. [10] performed a similar study on a larger sample, focusing specifically on time evolution of lags, and also found no consistent evolution trend. By contrast, Hakkila et al. [9] considered pulses from a sample of bursts with known redshift and found a robust lag–luminosity correlation resembling that of Norris et al. [15]. The present work develops a method for evaluating the lag–luminosity relationship in time-resolved lags without known redshifts or the ability to compare pulses between bursts.

Chapter 2

Methods

2.1 Burst selection

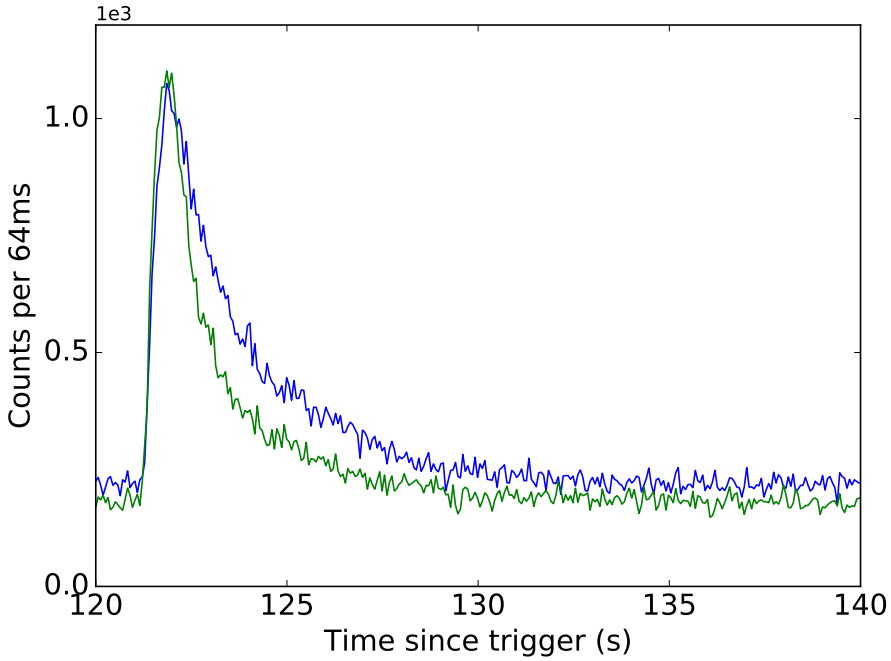

Figure 2.1: GRB 951016, a typical fast-rise-exponential-decay light curve; these events were excluded from analysis

We surveyed *BATSE* bursts from the public archive[1] in descending order on the CMAXMIN table, which orders triggers by peak count rate relative to the trigger rate. This method finds bursts with a high signal-to-noise ratio, which offer better precision in the cross-correlation analysis. We examined the top 150 entries in the table and eliminated short bursts ($T_{90} < 2$ s) and those consisting of one or two pulses without other significant features, which are unsuitable for the time-resolved lag analysis. The final sample included 42 *BATSE* bursts, of which 20 had three or more isolable pulses.

[1] `ftp://heasarc.gsfc.nasa.gov/compton/data/batse/`

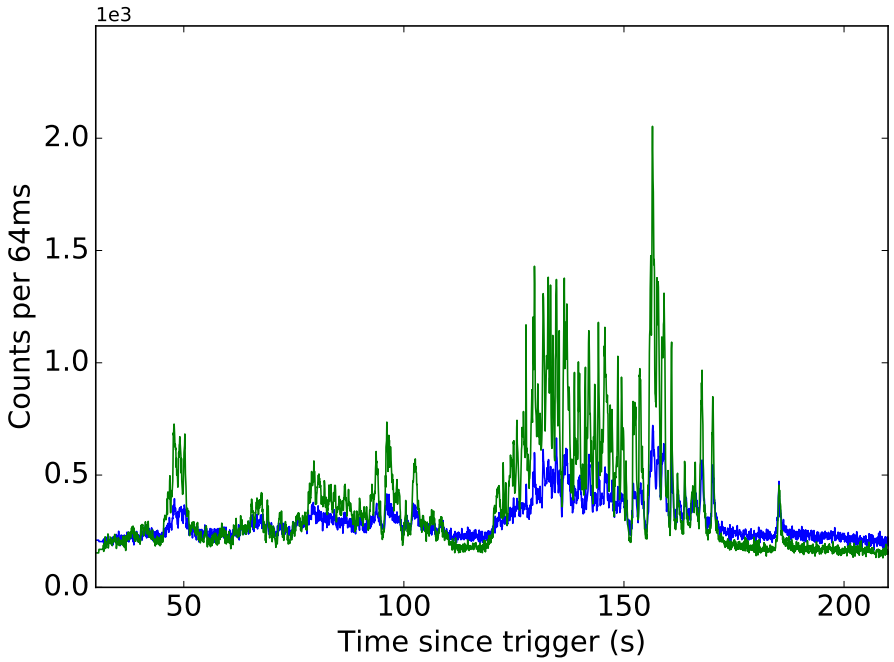

Figure 2.2: Typical light curve of burst with complex features, but without distinct pulses ("overlap" in Table 2.1)

2.2 Data preparation

2.2.1 Data format

BATSE produces three main data types: a continuous, low-rate stream which is recorded regardless of trigger status (DISCLA); a 64 ms resolution stream covering the 2.048 s before a trigger event (PREB); and another 64 ms resolution stream which records for 4–11 minutes after the trigger event (DISCSC) and generally contains the majority of the burst [1].

NASA's public FTP archive stores BATSE data as ASCII text files, as shown in Table 2.1. The first two lines give column headings and metadata: the BATSE trigger number, the number of points in the dataset, the duration of DISCLA data before PREB starts, and the amount of overlap between DISCLA and PREB.

Table 2.1: First four lines of a typical BATSE data file

```
trig#  npts nlasc 1preb    followed by 4-chan count rates (64-ms bins)
 3001  8187  1856     0
 2.18937500E+02  1.62687500E+02  1.17437500E+02  7.22500000E+01
 2.18937500E+02  1.62687500E+02  1.17437500E+02  7.22500000E+01
```

2.2.2 Slice formation

In the cases where a burst exhibited three or more distinct pulses, we created slices isolating individual pulses by multiplication with a Gaussian centered on the pulse peak with FWHM

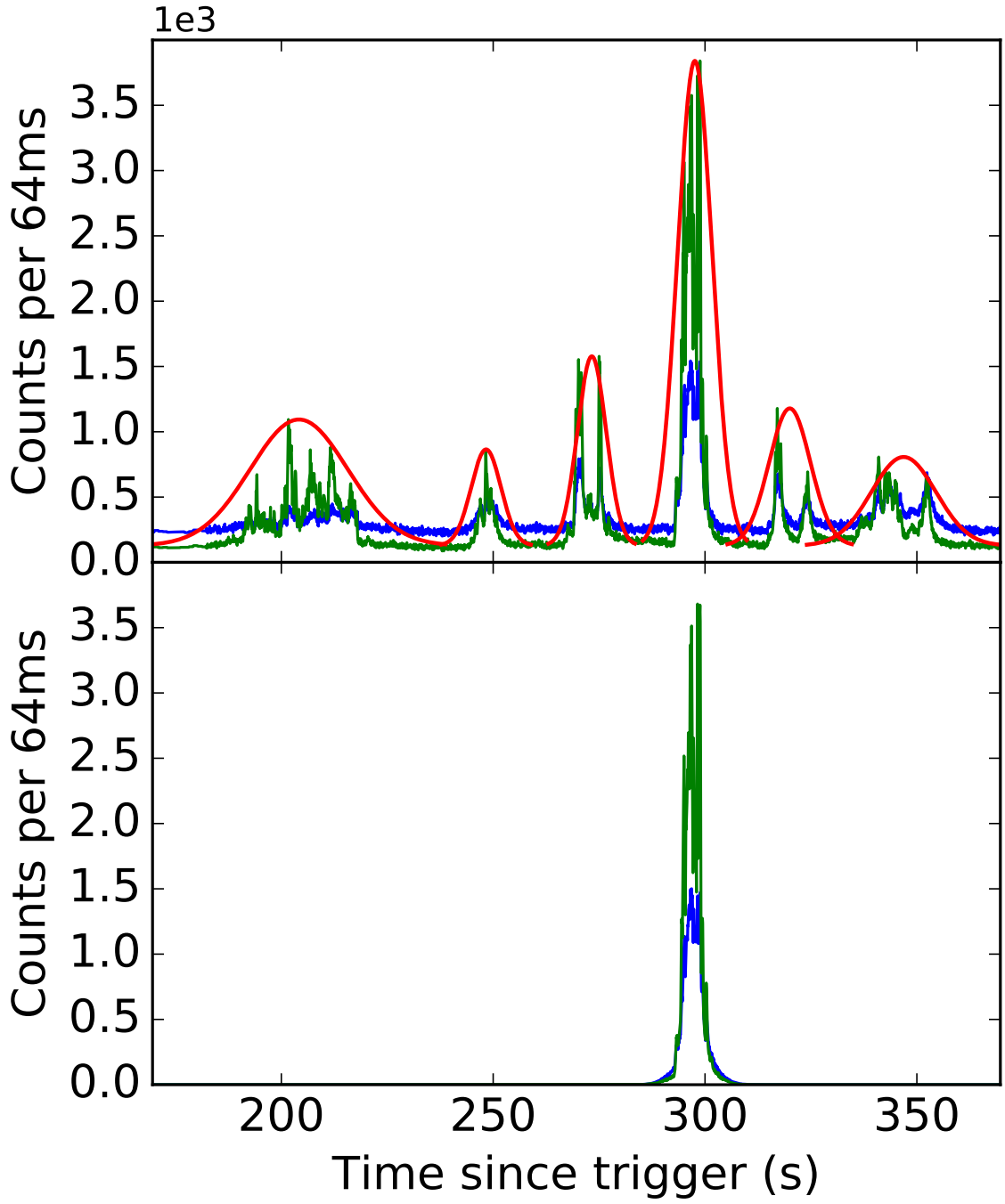

Figure 2.3: Upper panel: Light curve of pulsed GRB 940217 with Gaussian filters (Gaussian height exaggerated and vertical offset added for visibility); Lower panel: Isolated pulse after Gaussian filter (blue: ch1, green: ch3, red: Gaussian filter)

approximating the pulsewidth. Where isolable pulses were not present, but the light curve retained discernible features, we made three slices of the T_{90} interval by the previously-described method with evenly spaced centers and widths one-third of the T_{90}. For the cross-correlation analysis, each slice was trimmed to 10σ from the center of the Gaussian, where σ is the width parameter of the Gaussian. Fig. 2.3 illustrates the slicing process.

Since the bulk of the *BATSE* data lacks redshifts, we used the peak count rate summed over the channels as an approximation to the luminosity for lag correlation. This is appropriate as we do not attempt to compare lags or luminosities between bursts and are only interested in the relative intensity of pulses within individual bursts.

The *BATSE* DISCSC data carries information in four channels defined by photon energy range. The channels of interest for lag calculation are Channel 1 (25–55 keV) and Channel 3 (110–320 keV), where positive lag is defined as Channel 1 following Channel 3.

2.3 Analysis

2.3.1 Cross-correlation

The cross-correlation of two functions or data series over a common domain measures the similarity between the functions/series after one is shifted by an amount τ. If the series are identical with some shift τ_0 between them, the cross-correlation function is maximal when $\tau = \tau_0$ (or $\tau = -\tau_0$, depending on sign convention). This makes the cross-correlation an invaluable tool in signal analysis applications where one signal is expected to be simply a delayed version of another; in this case, the peak in the cross-correlation easily distinguishes the amount of this shift. This is exactly the case in GRB data, where the high- and low-energy channels have very similar time profiles up to the delay introduced by spectral lag.

2.3.1.1 Continuous

For (possibly complex) functions f and g defined on the real line, the cross-correlation $f \star g$ is given by

$$(f \star g)(\tau) = \int_{-\infty}^{\infty} f^*(t) g(t+\tau)\,\mathrm{d}t, \tag{2.1}$$

where $f^*(t)$ is the complex conjugate of f. This form showcases the basic principle of the cross-correlation: shift one input by τ, then compute the inner product between the inputs. In general, inner products measure the similarity of two vectors, which are in this case members of a vector space of functions on which the inner product takes the form of an integral. The idea is the same as the dot product of Euclidean vectors, where we multiply component-wise and then add the products. This definition is perfectly adequate for functions, but actual data is given on a finite lattice, not a continuum, so we need a different definition to compute lags effectively.

2.3.1.2 Discrete

We adopt the discrete cross-correlation defined by Band [2] and used in similar lag studies [3], which is defined by

$$\mathrm{CCF}(f, g, \tau) = \frac{\sum_i f_i g_{i+\tau}}{\sqrt{\sum_i f_i^2 \sum_i g_{i+\tau}^2}}. \tag{2.2}$$

This is certainly less intuitive than (2.1), but it is necessarily so due to the difficulty of accommodating finite, discrete data. A particular issue is that with finite data sets, shifting by τ entries leaves "tails" of length τ hanging off of each series which have no partner to multiply with. Thus, the number of elements contributing to the cross-correlation gets smaller and smaller as τ increases, dragging down the CCF even if the shifted series are becoming more similar. One resolution, which is appropriate for samples of periodic signals, is simply to glue the tails together and treat the data as circular. However, gamma-ray bursts are transient events and periodicity is very rare, so it is more reasonable to normalize each point in a way which accounts for the decreasing sample size; this is the purpose of the denominator in the definition. By construction, the normalized cross-correlation is exactly 1 at any τ where the series are identical.

2.3.2 Curve fitting

Because the discrete cross-correlation steps through the data point by point, the time-resolution of its output cannot be any finer than the input data. Since lags are typically on the order of 1–1000 ms while the BATSE data has a resolution of 64 ms, we cannot determine short lags with any precision simply by finding the maximum point of the CCF output. Thus, as seen in Fig. 2.4, we fit a curve to the CCF points near the peak and find its maximum to measure lags more finely than 64 ms. We used SciPy's `curve_fit` routine, which uses the Levenburg–Marquardt algorithm to fit arbitrary functions to given data.

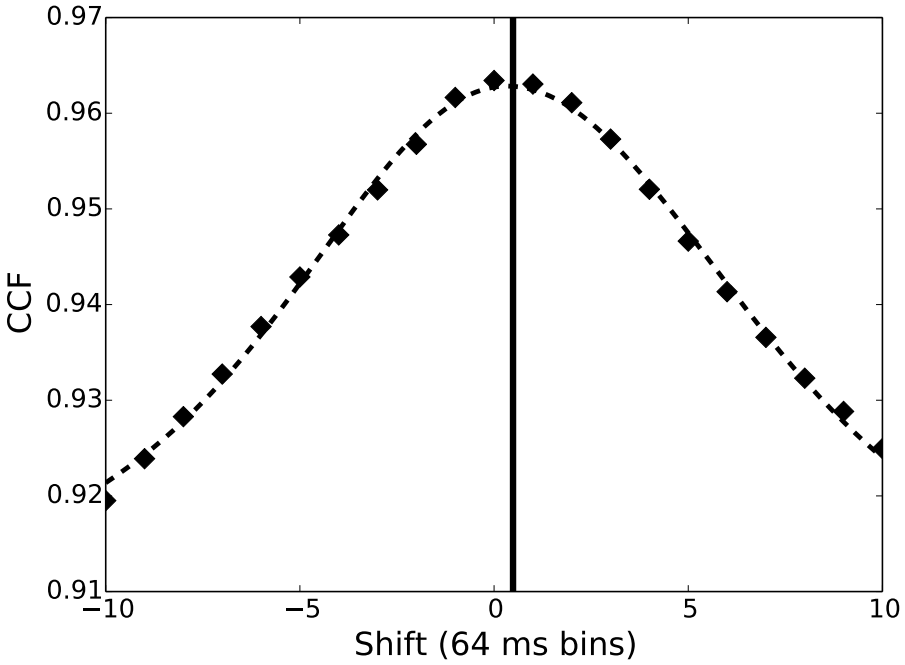

Figure 2.4: CCF of the second pulse in GRB 940217 with fit line; vertical line indicates fitted lag (uncertainty too small to represent in this figure)

2.3.2.1 Fit function

We used the function

$$f(\tau) = c + d_1 \exp\left(-\frac{\tau^2}{2\sigma_s^2}\right) + d_2 A(\tau) \tag{2.3}$$

for fitting, where σ_s is the width parameter of the slice under consideration and the function A is the asymmetric Gaussian

$$A(\tau) = \begin{cases} \exp\left(-\frac{(\tau-\tau_0)^2}{2\sigma_\ell^2}\right) & : \ \tau < \tau_0 \\ \exp\left(-\frac{(\tau-\tau_0)^2}{2\sigma_r^2}\right) & : \ \tau \geqslant \tau_0 \end{cases}, \tag{2.4}$$

giving c, d_1, d_2, τ_0, σ_ℓ, and σ_r as the free parameters. The asymmetric Gaussian is proposed by Bernardini et al. [3] to better fit the correlation profile produced by GRBs, since light curves of pulses are generally not themselves symmetric. We include the fixed-width Gaussian centered at zero because the Gaussian filter used to create each slice causes a fictitious correlation centered at $\tau = 0$ with width roughly that of the filter. Fitting for this separately improves the fit to the signal.

2.3.2.2 Fit range

We fit a range of points around the maximum with endpoints determined by the behavior of the CCF. Because many light curves contain several episodes whose shapes are similar, at long delays it is possible for pulses in the high-energy channel to align with *unrelated* pulses in the low-energy channel, which produces subsidiary maxima in the CCF. These do not reflect the phenomenon of spectral lag, so we must exclude them when fitting the cross-correlation data.

In cases of particularly noisy bursts where peaks are less sharply defined, the CCF can also have considerable noise, which may confound the fitting procedure. In these instances, we binned the points into averaged groups of 2 to 4 to get a smoother, but lower-resolution set for fitting.

2.3.3 Monte Carlo error estimation

Due to background noise and the noise intrinsic to the burst emission itself, there is a degree of uncertainty in each lag measured by the CCF fitting process. This uncertainty is not constant across bursts; the cross-correlation of some bursts exhibits great sensitivity to noise, while others are relatively insensitive. We employ a Monte Carlo bootstrap method to estimate this lag uncertainty for each burst. To do this, we simulate random variations of the light curve and determine the variance of the lags in response. Because radiation counting is a Poisson process, our approach is to treat each point of the light curve as a Poisson random variable whose expectation value is the measured rate at that point. We create 10,000 different light curves by sampling the Poisson distribution at each point, then perform the slicing, cross-correlation, and fitting procedures as above. This gives us 10,000 fitted lags for each slices; we use the mean lag for each slice and take the standard deviation of the sample as the uncertainty.

In some slices, this variation created wildly divergent CCFs which `curve_fit` was unable to fit. We eliminated any burst in which one slice experienced 1,000 or more such errors, as this could compromise the statistical validity of the bootstrap method.

2.3.4 Slope fitting

Because the majority of *BATSE* measurements predate effective burst localization methods, very few have confirmed redshifts, making it impossible to account for time dilation in the measured lags or determine isotropic luminosity to make direct comparisons between bursts. However, with a minimum of three data points for each burst, it is possible to determine trends across the slices of each burst and look for general consistency in the sample. In particular, we expect that the contributions of the unknown parameters have random — rather than systematic — impacts on the measured lag–luminosity relation which will balance out in the mean.

For each burst, we fit a straight line to the lag–luminosity data in log–log space. This corresponds to a power-law relationship in linear space: if we have

$$\log y = a \log x + c, \tag{2.5}$$

then

$$y = 10^c x^a. \tag{2.6}$$

This is the form of the correlation described by Norris et al. [15] and others, so we fit for this relationship. We take the relative uncertainty of each lag as an estimator of the uncertainty in its logarithm for fitting. This is not an ideal estimation in the cases where the relative uncertainty exceeds unity, but at worst this leads to an underconfident fit, not an overconfident one. For data where the mean lag is negative (and thus can't be plotted on logarithmic axes), but the 1σ interval includes positive values, we use the point as an upper bound and fit as if it were positive with the same upper uncertainty limit as the original point.

In order to determine uncertainties on the slopes of the fitted lines, we vary the intercept parameter and refit the slope until the χ^2 statistic (a goodness-of-fit metric) exceeds that of the best-fit line by 1. This process constructs a range of slopes which give an acceptable fit to the data, and we use the width of this interval to estimate the error in the best-fit slope.

When one point has significantly wider error bars than the rest, it is possible for the fitting routine to disregard it almost entirely, since the contribution of each point to the fit is weighted by its variance. If only three points are being fit in total, this can lead to a line determined essentially by two points, which, needless to say, is not a result. Thus, we visually examine the fit line for each burst and reject any exhibiting such a two-point fit.

Chapter 3

Results and Discussion

Of the initial survey of 150 candidate bursts, we obtained slopes with uncertainties for 31 bursts, of which 14 exhibited three or more distinguishable pulses. The slopes and their uncertainties are tabulated along with morphological category and T_{90} in Table 3.1, while Figure 3.1 displays these data as a scatter plot and the histogram in Figure 3.2 illustrates their distribution.

By visual inspection, we divided our sample into three morphological categories: bursts with indistinct or overlapping pulses (denoted "overlap" in Table 3.1), bursts with one or more precursors before a main pulse (denoted "precursor" in Table 3.1), and bursts with multiple distinct pulses (denoted "pulsed" in Table 3.1). Before computing statistics on these results, we may get a rough overview by making a few observations. First, on a purely qualitative level, the mass of the histogram appears concentrated slightly to the left of zero, though without uncertainty the significance of this is unclear.

Second, by counting points in Figure 3.1, we see 7 positive slopes (5 overlap, 1 with precursor, 1 with pulses), 10 negative slopes (3 overlap, 7 with pulses), and 14 slopes (9 overlap, 1 with precursor, 4 with pulses) which are consistent with zero (i.e. the error bars cross the x-axis). The pulsed bursts appear to have a lag paradigm distinct from the overlap or precursor bursts, so it is sensible to analyze them as a subsample.

3.1 Weighted mean

The weighted mean is a useful summary statistic for data where some points should be given preference over others. In general, for a set of data $\{x_1, \ldots, x_n\}$ with a set of weights $\{w_1, \ldots, w_n\}$, the weighted mean is

$$\bar{x} = \frac{\sum_{i=1}^{n} w_i x_i}{\sum_{i=1}^{n} w_i}. \tag{3.1}$$

Note that if the weights are normalized, the denominator becomes unity. If all of the weights are the same, we recover the familiar unweighted mean. Much as in the unweighted case, it is possible to estimate the variance of the weighted mean when the data being averaged have uncertainties. This variance is

$$\sigma_{\bar{x}}^2 = \frac{\sum_{i=1}^{n} w_i^2 \sigma_i^2}{\left(\sum_{i=1}^{n} w_i\right)^2}, \tag{3.2}$$

where σ_i^2 is the variance of the datum x_i.

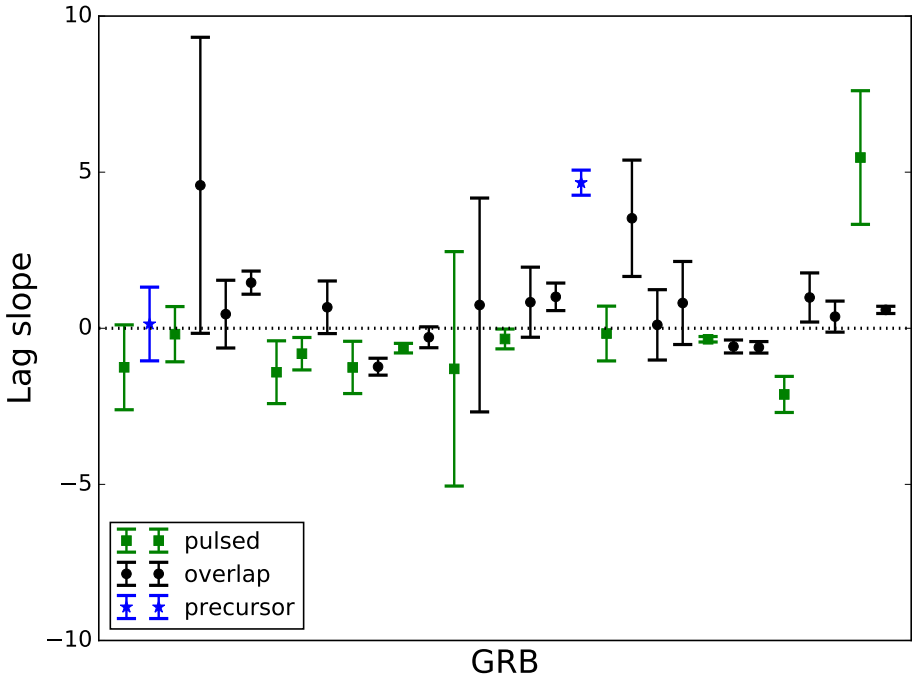

Figure 3.1: Scatter plot of computed lag slopes with uncertainty, ordered by burst date; dotted line marks zero level

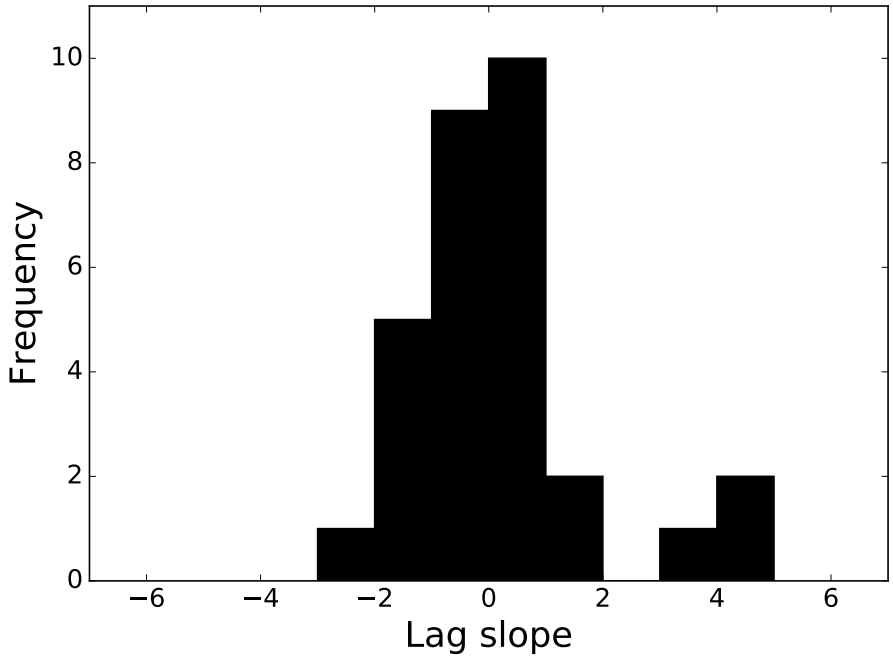

Figure 3.2: Histogram of computed lag slope values; note that uncertainty cannot be represented

Table 3.1: GRBs included in final analysis. Columns: burst name, T90, morphology, number of slices, lag slope, uncertainty in slope (σ).

Name	T90 (s)	Category	Slices	Slope	σ
910522	29.7	Pulsed	5	−0.815	0.519
910619	106.1	Overlap	3	3.523	1.863
910717	4.9	Overlap	3	0.109	1.127
920110	318.6	Pulsed	6	−1.250	1.359
920221	10.4	Precursor	5	0.137	1.181
920226	24.4	Pulsed	3	−0.189	0.884
920406	26.2	Overlap	3	4.579	4.741
920513	88.6	Overlap	3	0.453	1.085
920525	16.1	Overlap	3	1.462	0.370
930201	154.4	Pulsed	3	−1.407	1.006
930309	90.1	Overlap	3	0.672	0.843
931014	12.9	Pulsed	5	−1.254	0.837
940210	30.7	Overlap	3	−1.231	0.271
940217	150.1	Pulsed	6	−0.637	0.153
940302	119.9	Overlap	3	−0.289	0.335
940619	88.4	Pulsed	4	−1.299	3.755
940817	32.2	Overlap	3	0.746	3.425
941014	45.4	Pulsed	8	−0.342	0.318
941017	77.1	Overlap	3	0.835	1.123
941023	34.9	Overlap	3	1.007	0.441
941121	43.6	Precursor	3	4.664	0.402
951203	172.7	Pulsed	3	−0.168	0.877
960815	12.8	Overlap	3	0.810	1.330
970201	26.9	Pulsed	4	−0.352	0.087
970315	16.8	Overlap	3	−0.584	0.207
970420	10.5	Overlap	3	−0.610	0.184
980105	36.8	Pulsed	6	−2.119	0.578
980124	45.1	Overlap	3	0.986	0.786
980803	19.8	Overlap	3	0.373	0.497
980828	22.2	Pulsed	3	5.469	2.140
980923	33.0	Overlap	3	0.589	0.116

In the present case, we use the uncertainties of the slope data as weights to produce a mean which favors more precise data over data with large error bars. Specifically, for a data set $\{x_1, \ldots, x_n\}$ with standard deviations $\{\sigma_1, \ldots, \sigma_n\}$, we define the weighted mean as

$$\bar{x} = \frac{\sum_{i=1}^{n} x_i \sigma_i^{-2}}{\sum_{i=1}^{n} \sigma_i^{-2}}, \tag{3.3}$$

so that the weight of each point is the reciprocal of its variance. This ensures that measurements with high variance have low weight and vice versa. The variance of the mean is then

$$\sigma_{\bar{x}}^2 = \frac{\sum_{i=1}^{n} \sigma_i^{-4} \sigma_i^2}{\left(\sum_{i=1}^{n} \sigma_i^{-2}\right)^2} = \frac{\sum_{i=1}^{n} \sigma_i^{-2}}{\left(\sum_{i=1}^{n} \sigma_i^{-2}\right)^2} = \frac{1}{\sum_{i=1}^{n} \sigma_i^{-2}}, \tag{3.4}$$

and we can take the square root of this variance as the uncertainty in the mean.

Using these definitions, we calculate for the full sample of 31 bursts a weighted mean slope of -0.117 ± 0.052. The subset of bursts with overlapping bursts has mean slope 0.09 ± 0.08 (no significant correlation), while the sample with precursors shows a weighted mean of 4.2 ± 0.4. The latter result, while apparently significant, is based on too small a sample to draw any conclusions.

When we restrict our attention to the subsample of bursts with multiple distinct pulses, however, the weighted mean becomes -0.455 ± 0.071. This result exhibits 6σ significance.

3.2 Conclusions

Over a sample of 31 BATSE light curves, our time-resolved cross-correlation analysis faintly suggests a negative lag–luminosity correlation across episodes within long GRBs. However, our sample comprises three distinct populations which appear to belong to different lag regimes.

In the subsample with overlapping pulse features we find no significant correlation. The two bursts with precursors average to a significant positive correlation, but the size of the sample makes it statistically unreliable. Lastly, the set of 12 bursts with multiple distinct pulses exhibits a highly significant negative correlation.

The small size of our total sample — and of the subsample showing a strong correlation — limits the confidence of any conclusions drawn, but our results support the possibility that the lag–luminosity correlation among full bursts extends to pulses within bursts, at least where those pulses are well-separated in time. A natural sequel to this work would be to further automate the analysis and consider a much larger sample, especially one from a modern instrument such as Fermi which offers higher data resolution.

Acknowledgments

I would like first to thank my advisor, Dr. Davide Lazzati, for his guidance, support, and expertise throughout this lengthy, stubborn project. I wish also to thank Dr. David Roundy and Dr. Kathryn Hadley for participating in my thesis defense, my classmates for their constructive feedback on many drafts, and Dr. Janet Tate for motivating me to a frankly unprecedented level of productivity. Lastly, I would like to thank Lauren Pittis and Kalia Flocker for their utterly undeserved degree of patience and kindness during this year of stress and angst.

Bibliography

[1] Concatenated 64-ms burst data in ASCII format. ftp://legacy.gsfc.nasa.gov/compton/data/batse/ascii_data/64ms/README. Accessed: 2016-02-29.

[2] D. L. Band. Gamma-Ray Burst Spectral Evolution through Cross-Correlations of Discriminator Light Curves. *The Astrophysical Journal*, 486(2):928, Sept. 1997. ISSN 0004-637X. doi: 10.1086/304566. URL http://iopscience.iop.org/0004-637X/486/2/928.

[3] M. G. Bernardini, G. Ghirlanda, S. Campana, S. Covino, R. Salvaterra, J.-L. Atteia, D. Burlon, G. Calderone, P. D'Avanzo, V. D'Elia, G. Ghisellini, V. Heussaff, D. Lazzati, A. Melandri, L. Nava, S. D. Vergani, and G. Tagliaferri. Comparing the spectral lag of short and long gamma-ray bursts and its relation with the luminosity. *Monthly Notices of the Royal Astronomical Society*, 446(2):1129–1138, Nov. 2014. ISSN 0035-8711, 1365-2966. doi: 10.1093/mnras/stu2153. URL http://arxiv.org/abs/1410.5216. arXiv: 1410.5216.

[4] H.-Y. Chang. Correlation Between Collimation-Corrected Peak Luminosity and Spectral Lag of Gamma-ray Bursts in the Source Frame. *Journal of Astronomy and Space Sciences*, 29(3):253–258, Sept. 2012. ISSN 2093-5587. doi: 10.5140/JASS.2012.29.3.253. URL http://koreascience.or.kr/journal/view.jsp?kj=OJOOBS&py=2012&vnc=v29n3&sp=253.

[5] L. Chen, Y. Q. Lou, M. Wu, J. L. Qu, S. M. Jia, and X. J. Yang. Distribution of Spectral Lags in Gamma Ray Bursts. *The Astrophysical Journal*, 619(2):983–993, Feb. 2005. ISSN 0004-637X, 1538-4357. doi: 10.1086/426774. URL http://arxiv.org/abs/astro-ph/0410344. arXiv: astro-ph/0410344.

[6] L. X. Cheng, Y. Q. Ma, K. S. Cheng, T. Lu, and Y. Y. Zhou. The time delay of gamma-ray bursts in the soft energy band. *Astronomy and Astrophysics*, 300:746, Aug. 1995. ISSN 0004-6361. URL http://adsabs.harvard.edu/abs/1995A%26A...300..746C.

[7] G. J. Fishman and C. A. Meegan. Gamma-Ray Bursts. *Annual Review of Astronomy and Astrophysics*, 33(1):415–458, 1995. doi: 10.1146/annurev.aa.33.090195.002215. URL http://dx.doi.org/10.1146/annurev.aa.33.090195.002215.

[8] N. Gehrels, E. Ramirez-Ruiz, and D. Fox. Gamma-Ray Bursts in the Swift Era. *Annual Review of Astronomy and Astrophysics*, 47(1):567–617, 2009. doi: 10.1146/annurev.astro.46.060407.145147. URL http://dx.doi.org/10.1146/annurev.astro.46.060407.145147.

[9] J. Hakkila, T. W. Giblin, J. P. Norris, P. C. Fragile, and J. T. Bonnell. Correlations Between Lag, Luminosity, and Duration in Gamma-ray Burst Pulses. *The Astrophysical Journal*, 677(2):L81–L84, Apr. 2008. ISSN 0004-637X, 1538-4357. doi: 10.1086/588094. URL http://arxiv.org/abs/0803.1655. arXiv: 0803.1655.

[10] L. Jia, T. Yi, and E. Liang. Spectral lags in different episodes of gamma-ray bursts. *Science China Physics, Mechanics and Astronomy*, 56(8):1437–1442, June 2013. ISSN 1674-7348, 1869-1927. doi: 10.1007/s11433-013-5149-7. URL http://link.springer.com/article/10.1007/s11433-013-5149-7.

[11] R. W. Klebesadel, I. B. Strong, and R. A. Olson. Observations of Gamma-Ray Bursts of Cosmic Origin. *The Astrophysical Journal Letters*, 182:L85, June 1973. ISSN 0004-637X. doi: 10.1086/181225. URL http://adsabs.harvard.edu/abs/1973ApJ...182L..85K.

[12] T. P. Li, J. L. Qu, H. Feng, L. M. Song, G. Q. Ding, and L. Chen. Timescale Analysis of Spectral Lags. *Chinese Journal of Astronomy and Astrophysics*, 4(6):583–598, Dec. 2004. ISSN 1009-9271. doi: 10.1088/1009-9271/4/6/583. URL http://arxiv.org/abs/astro-ph/0407458. arXiv: astro-ph/0407458.

[13] R. Margutti, C. Guidorzi, G. Chincarini, M. G. Bernardini, F. Genet, J. Mao, and F. Pasotti. Lag-luminosity relation in gamma-ray burst X-ray flares: a direct link to the prompt emission. *Monthly Notices of the Royal Astronomical Society*, 406(4):2149–2167, Aug. 2010. ISSN 00358711. doi: 10.1111/j.1365-2966.2010.16824.x. URL http://arxiv.org/abs/1004.1568. arXiv: 1004.1568.

[14] J. P. Norris. Implications of the Lag-Luminosity Relationship for Unified Gamma-Ray Burst Paradigms. *The Astrophysical Journal*, 579(1):386, Nov. 2002. ISSN 0004-637X. doi: 10.1086/342747. URL http://iopscience.iop.org/0004-637X/579/1/386.

[15] J. P. Norris, G. F. Marani, and J. T. Bonnell. Connection between Energy-dependent Lags and Peak Luminosity in Gamma-Ray Bursts. *The Astrophysical Journal*, 534(1):248, May 2000. ISSN 0004-637X. doi: 10.1086/308725. URL http://iopscience.iop.org/0004-637X/534/1/248.

[16] T. N. Ukwatta, K. S. Dhuga, M. Stamatikos, T. Sakamoto, W. C. Parke, S. D. Barthelmy, and N. Gehrels. The lag-luminosity relation in the gamma-ray burst source-frame. *arXiv:1003.0229 [astro-ph]*, Feb. 2010. URL http://arxiv.org/abs/1003.0229. arXiv: 1003.0229.

[17] J. van Paradijs, C. Kouveliotou, and R. A. M. J. Wijers. Gamma-Ray Burst Afterglows. *Annual Review of Astronomy and Astrophysics*, 38(1):379–425, 2000. doi: 10.1146/annurev.astro.38.1.379. URL http://dx.doi.org/10.1146/annurev.astro.38.1.379.

[18] S. Woosley and J. Bloom. The Supernova–Gamma-Ray Burst Connection. *Annual Review of Astronomy and Astrophysics*, 44(1):507–556, 2006. doi: 10.1146/annurev.astro.43.072103.150558. URL http://dx.doi.org/10.1146/annurev.astro.43.072103.150558.

[19] Z. B. Zhang, H. C. Liu, L. Y. Jiang, and D. Y. Chen. Different Luminosity Correlation of GRBs. *Journal of Astrophysics and Astronomy*, 35(3):561–564, Nov. 2014. ISSN 0250-6335, 0973-7758. doi: 10.1007/s12036-014-9287-8. URL `http://link.springer.com/article/10.1007/s12036-014-9287-8`.